Supporting Information

Vertically Aligned and Ordered Arrays of 2D MCo_2S_4@Metal with Ultrafast Ion/Electron Transport for Thickness-Independent Pseudocapacitive Energy Storage

Zongbin Hao,[1,2] *Xingchen He,*[1,2] *Hongdou Li,*[1,2] *Denis Trefilov,*[1,2] *Yangyang Song,*[1,2] *Yang Li,*[1,2] *Xinxin Fu,*[1,2] *Yushuang Cui,*[1,2] *Shaochun Tang,**[1,2] *Haixiong Ge,**[1,2] *Yanfeng Chen*[2]

[1] Department of Materials Science and Engineering, Collaborative Innovation Center of Advanced Microstructures, Jiangsu Key Laboratory of Artificial Functional Materials, College of Engineering and Applied Sciences, Nanjing University, Nanjing 210093, P. R. China

[2] National Laboratory of Solid State Microstructures, Nanjing 210093, China.

E-mails: tangsc@nju.edu.cn (S.T.) or haixiong@nju.edu.cn (H.G.)

Figure Captions in Supporting Information

Figure S1. Illustration of synthesis process of a nickel template.

Figure S2. XRD patterns of the typical $NiCo_2S_4$@NC-array and the bare NC-array.

Figure S3. XPS spectra of the typical 2D $NiCo_2S_4$@NC-array electrode.

Figure S4. SEM images of $FeCo_2S_4$ nanowires grown on NC-array, (a) top view SEM image, and (b) is local magnification of the selected area.

Figure S5. SEM images recorded from a vertical view showing ordered covered columns from the HS-5 and HS-7 samples.

Figure S6. Cross-section SEM images of (a) HS-7 and (b) HS-9 samples.

Figure S7. Electrochemical performance (a) CV curves and (b) GCD curves of the $NiCo_2S_4$@NC-array electrodes obtained with different t_R. CV curve of bare Ni substrates after acid treatment was provided for comparison.

Figure S8. A low-magnification SEM image recorded from a vertical view and EDS elemental mappings of different elements of Ni, Co, and S after 2000 cycles.

Figure S9. XPS analysis of the $NiCo_2S_4$@NC-array electrode after 2000 cycles.

Figure S10. (a) The microscopic morphology of a porous RGO film pressed on a Ni foam. (b) CV curves of the positive and negative electrodes recorded at 20 mV s^{-1}.

Table S1. Electrochemical performance comparison of our optimized $NiCo_2S_4$@NC-array electrode with recently reported $NiCo_2S_4$ arrays.

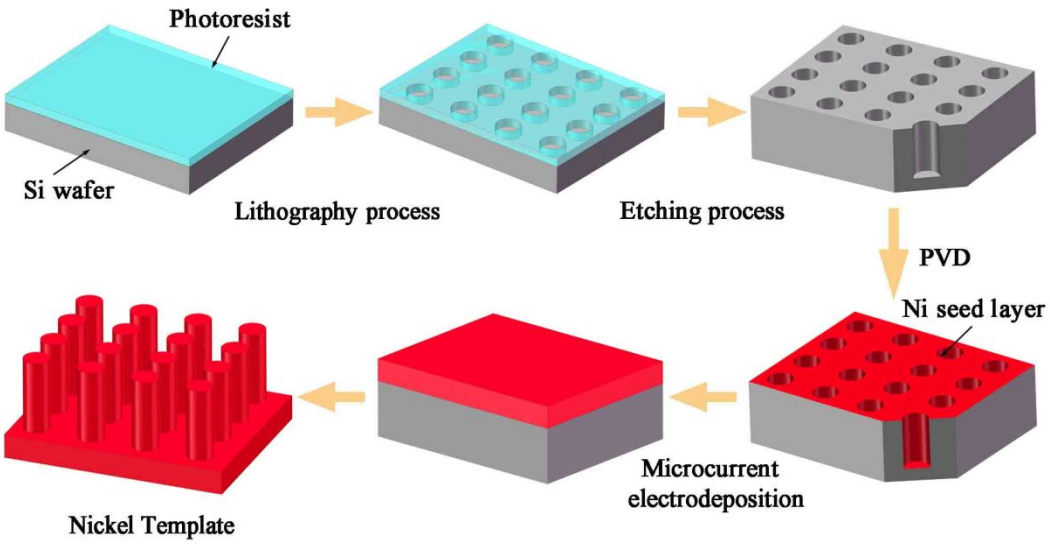

Figure S1. Illustration of synthesis process of a nickel template with a periodically ordered Ni column array starting from a Si wafer.

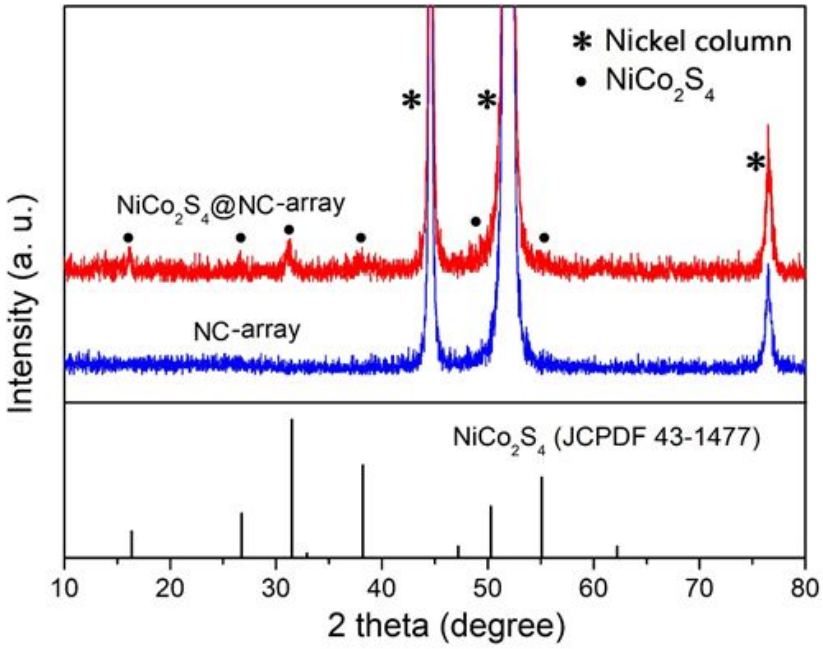

Figure S2. XRD patterns of the typical $NiCo_2S_4$@NC-array and the bare NC-array.

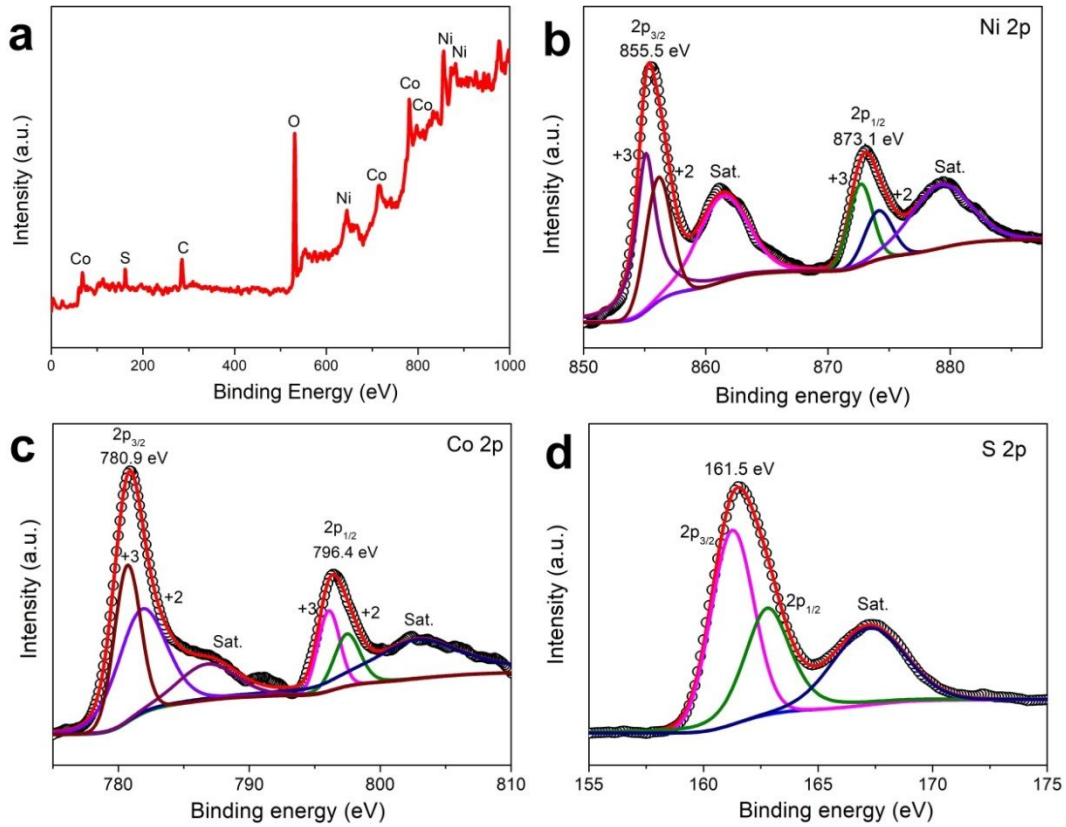

Figure S3. XPS spectra of the typical $NiCo_2S_4$@NC-array electrode. (a) A survey spectrum, and high-resolution spectra of (b) Ni 2*p*, (c) Co 2*p*, and (d) P 2*p*.

As seen from the X-ray diffraction (XRD) pattern (**Figure S2)**, several distinct peaks are observable (comparing with the bare Ni-array). The peaks at 16.3°, 26.7°, 31.6°, 38.3°, 50.1°, and 55° can be indexed to the (111), (220), (311), (400), (511), and (440) planes of the standard cubic $NiCo_2S_4$ phase (JCPDF No. 43-1477). The other three strong diffraction peaks are corresponding to those of nickel.

The elemental composition and chemical states were characterized by X-ray photoelectron spectra (XPS). The elements of Co, Ni and S can be easily identified through a survey spectrum (**Figure S3a**). Since XPS analysis collects information of several nanometers depth away from the outer surface of samples, it provided the element information from the surface active materials. The XPS results show that the surface element ratio is close to 1:2:4, which is consistent with the SEM-EDS result. Three kinds of elements were fitted using a Gaussian fitting method. Two significant peaks at binding energies of 855.5 and 873.1 eV are assigned to the Ni $2p_{3/2}$ and Ni$2p_{1/2}$, corresponding to the Ni^{2+} and Ni^{3+} (**Figure S3b**), accompanied by two shakeup satellites (indicated as "Sat"). From the Co2*p* spectrum, binding energies of 780.9 eV and 796.4 eV correspond to Co$2p_{3/2}$ and Co$2p_{1/2}$, which can be assigned to the signals of Co^{2+} and Co^{3+} (**Figure S3c**). In the S2p spectrum, the peaks at 161.3 eV and 162.8 eV correspond to the S$2p_{3/2}$ and S$2p_{1/2}$, and the peak at 167.4 eV is assigned as a shakeup satellite (**Figure S3d**). In a brief, the near-surface of the resulting nanosheet-covered array is comprised of Ni^{2+}/Ni^{3+}, Co^{2+}/Co^{3+}, and S^{2-}, which further demonstrates the generation of $NiCo_2S_4$ on NC-array. The XPS result is consistent with those from the XRD and TEM analysis.

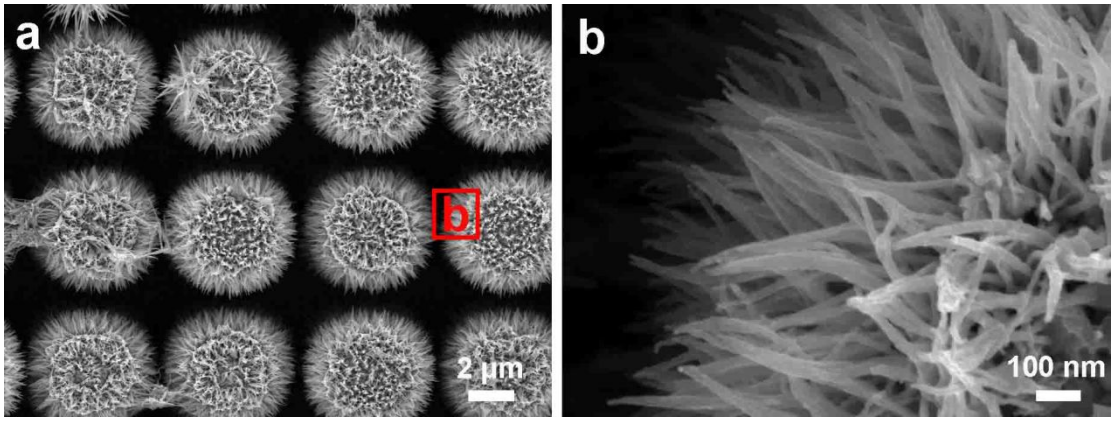

Figure S4. SEM images of $FeCo_2S_4$ nanowires grown on NC-array, (a) top view SEM image, and (b) is local magnification of the selected area.

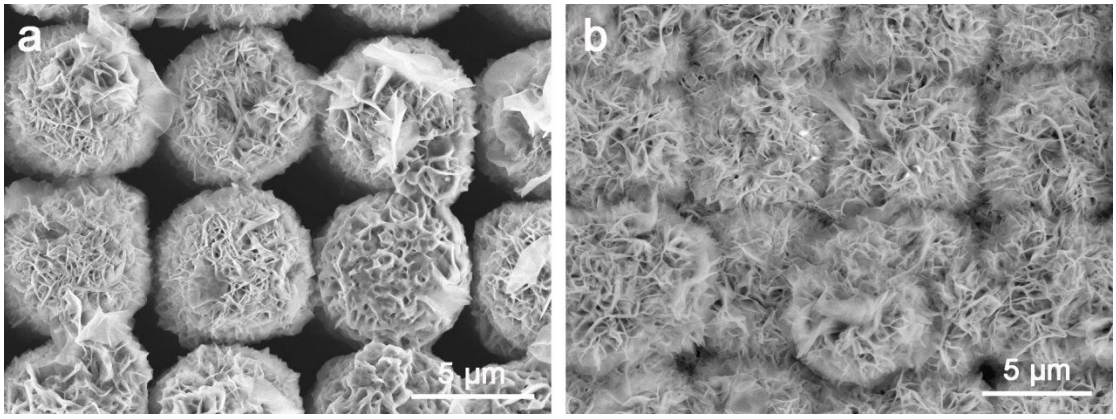

Figure S5. SEM images recorded from a vertical view showing ordered covered columns from the HS-5 and HS-7 samples.

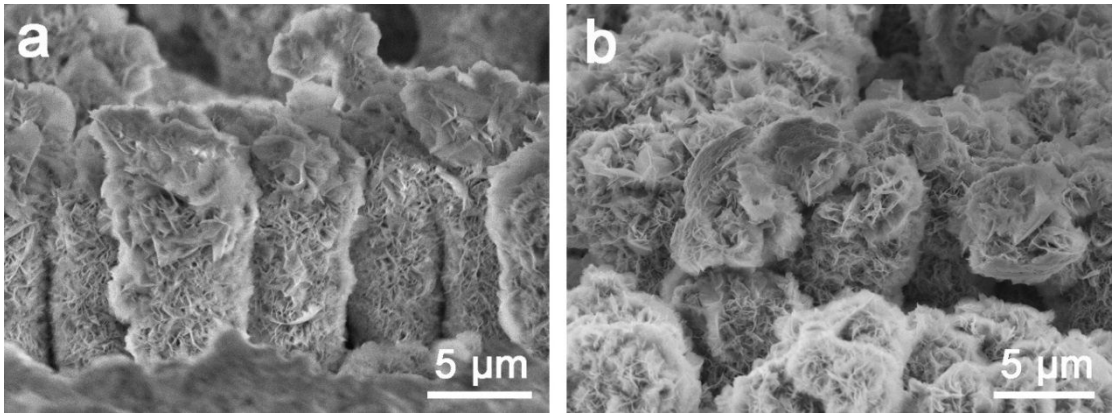

Figure S6. Cross-section SEM images of (a) HS-7 and (b) HS-9 samples.

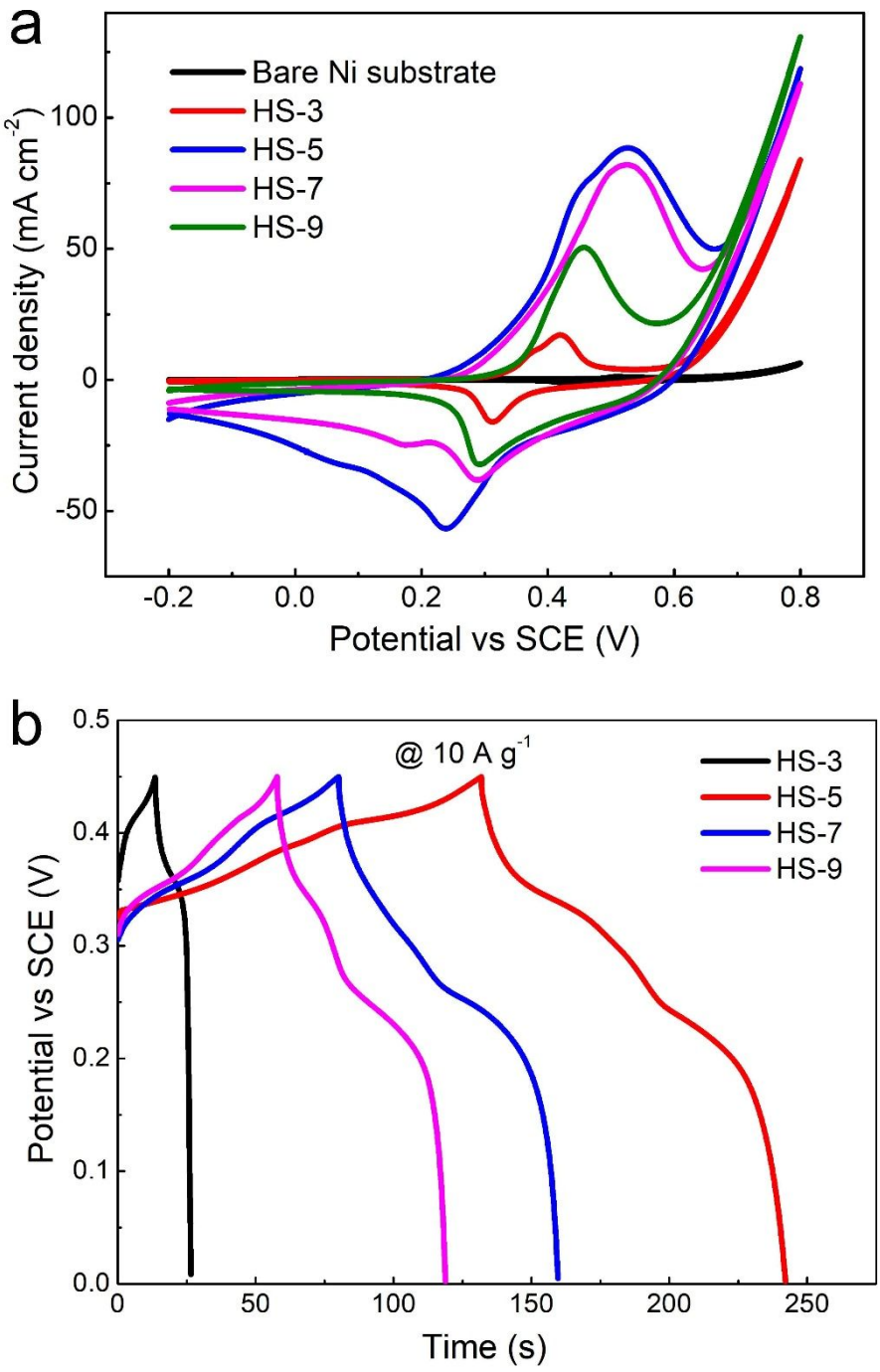

Figure S7. Electrochemical performance measurement results (a) CV curves of the $NiCo_2S_4$@NC-array electrodes obtained with different t_R of 3, 5, 7, and 9 h (corresponding to the HS-3, HS-5, HS-7, and HS-9 samples, respectively). CV curve of bare Ni substrates after acid treatment was provided for comparison. (b) GCD curves of the HS-3, HS-5, HS-7, and HS-9 samples, respectively).

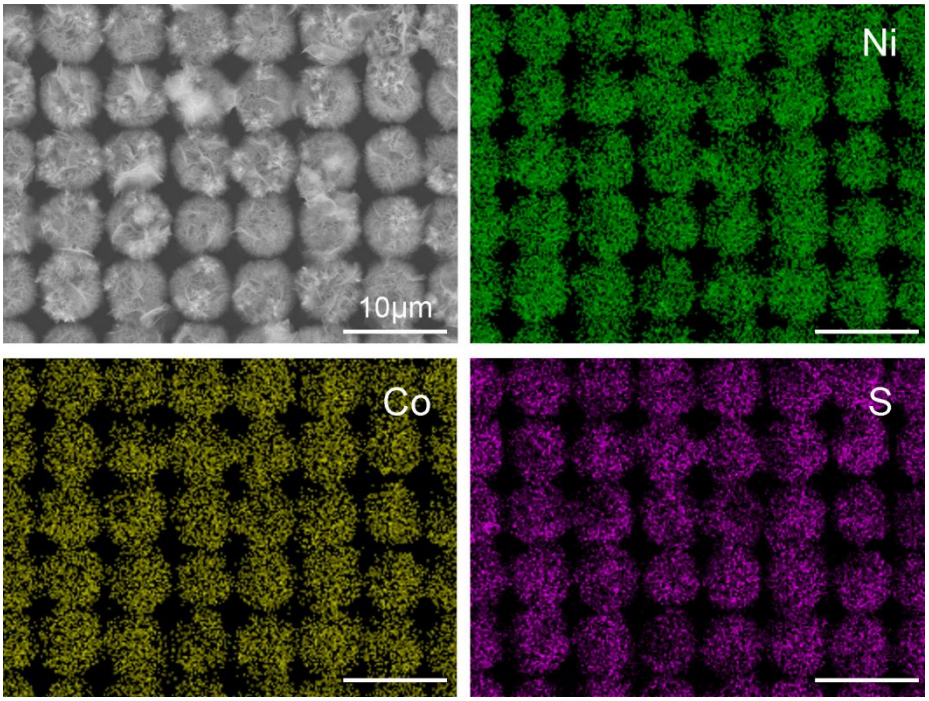

Figure S8. A low-magnification SEM image recorded from a vertical view and EDS elemental mappings of different elements of Ni, Co, and S after 2000 cycles.

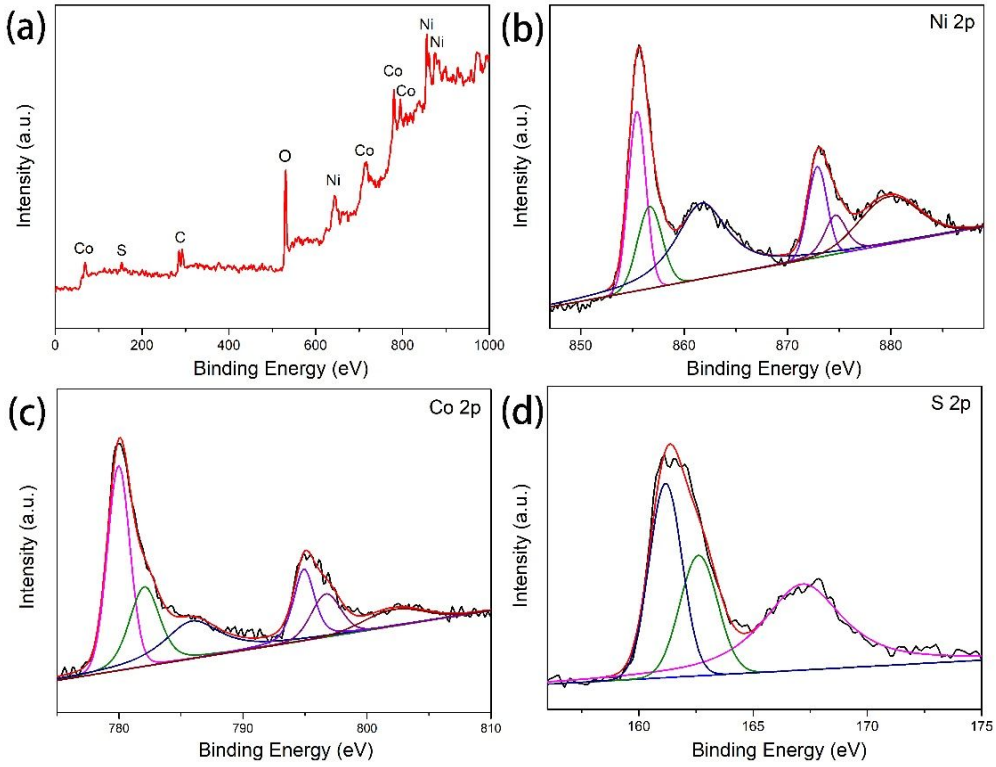

Figure S9. XPS analysis of the $NiCo_2S_4$@NC-array electrode after 2000 charge-discharge cycles (a) A survey spectrum, and high-resolution spectra of (b) Ni 2*p*, (c) Co 2*p*, and (d) P 2*p*, respectively.

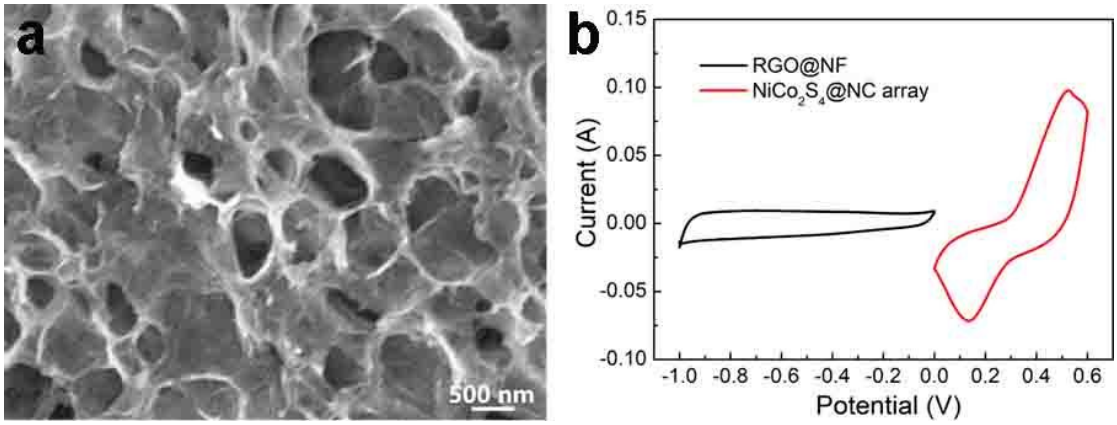

Figure S10. (a) The microscopic morphology of a porous RGO pressed on a Ni foam. (b) CV curves of the positive and negative electrodes recorded at 20 mV s^{-1}.

Table S1. Electrochemical performance comparison of our optimized $NiCo_2S_4$@NC-array electrode with recently reported $NiCo_2S_4$ arrays.

Materials	Electrolyte	Potential window	Specific Capacity	Rate Capability	Ref.
$Ni_xCo_{3-x}P_y$ Porous Nanowires	**3 M KOH**	**0-0.5 V**	**469** mAh g^{-1} at 2 A g^{-1}	**427** mAh g^{-1} (20 A g^{-1})	**44**
$CoNi_2S_4$ nanosheets	**2 M KOH**	**-0.1-0.65V**	**258** mAh g^{-1} at 1 A g^{-1}	**234** mAh g^{-1} (20 A g^{-1})	**54**
CNTs@Ni–Co–S nanosheet core/shell arrays	**2 M KOH**	**-0.2-0.6 V**	**222** mAh g^{-1} at 4 A g^{-1}	**106** mAh g^{-1} (50 A g^{-1})	**55**
Ni-Co-P	**2 M KOH**	**0-0.8 V**	**194** mAh g^{-1} at 1 A g^{-1}	**-**	**56**
Petal-like Ni–Co–S nanosheet	**1 M KOH**	**-0.2-0.6V**	**405** mAh g^{-1} at 1 A g^{-1}	**328** mAh g^{-1} (10 A g^{-1})	**57**
$NiCo_2S_4$ flaky arrays	**6M KOH**	**-0.1-0.5 V**	**284** mAh g^{-1} at 1 A g^{-1}	**145** mAh g^{-1} (8 A g^{-1})	**58**
$NiCo_2S_4$ nanosheet on graphene	**2 M KOH**	**0-0.5 V**	**202** mAh g^{-1} at 3 A g^{-1}	**106** mAh g^{-1} (20 A g^{-1})	**59**
$NiCo_2S_4$@NC array	**3 M KOH**	**0-0.45 V**	**487** mAh g^{-1} at 1 A g^{-1}	**150** mAh g^{-1} (100 A g^{-1})	**This work**